

Article

Visible-Light-Driven Bio-Templated Magnetic Copper Oxide Composite for Heterogeneous Photo-Fenton Degradation of Tetracycline

Olushola Adewole Alani ¹, Hadiza Abdullahi Ari ^{1,2}, Susanna Olushola Alani ³, Nnanake-Abasi O. Offiong ¹ and Wei Feng ^{1,*}

¹ Key Laboratory of Groundwater Resource and Environment, Ministry Education, College of New Energy and Environment, Jilin University, Changchun 130021, China; sholaw777@gmail.com (O.A.A.); haari@noun.edu.ng (H.A.A.); offiong18@mails.jlu.edu.cn (N.-A.O.O.)

² Faculty of Science, National Open University of Nigeria, Abuja 900211, Nigeria

³ Science Laboratory Department, Nigeria Institute of Leather and Science Technology, Zaria 810211, Nigeria; susannayaks@gmail.com

* Correspondence: weifeng@jlu.edu.cn; Tel.: +86-431-88502606

Abstract: The development of a visible-light-driven, reusable, and long-lasting catalyst for the heterogeneous photo-Fenton process is critical for practical application in the treatment of contaminated water. This study focuses on synthesizing a visible-light-driven heterogenous bio-templated magnetic copper oxide composite (Fe₃O₄/CuO/C) by a two-step process of bio-templating and hydrothermal processes. The prepared composite was characterized by field emission-scanning electron microscope (FE-SEM), Fourier-transform infrared spectroscopy (FTIR), thermogravimetric analysis (TGA), X-ray photoelectron spectroscopy (XPS), electrical impedance spectroscopy (EIS), and vibrating sample magnetometer (VSM). The results reveal that the prepared composite retains the template's (corn stalk's) original porous morphology, and a substantial amount of CuO and Fe₃O₄ particles are loaded onto the surface of the template. The prepared Fe₃O₄/CuO/C composite was employed as a catalyst for heterogeneous photo-Fenton degradation of tetracycline (TC) irradiated by visible light. The prepared Fe₃O₄/CuO/C catalyst has high efficiency towards TC degradation within 60 min across a wide pH range irradiated by visible light, which is attributed to its readily available interfacial boundaries, which significantly improves the movement of photoexcited electrons across various components of the prepared composite. The influence of other parameters such as initial H₂O₂ concentration, initial concentration of TC, and catalyst dosages was also studied. In addition to high efficiency, the prepared catalyst's performance was sustained after five cycles, and its recovery is aided by the use of an external magnetic field. This research paper highlights the development of a heterogeneous catalyst for the elimination of refractory organic compounds in wastewater.

Keywords: Fe₃O₄/CuO/C; bio-template; cornstalk; visible-light; photo-Fenton; tetracycline degradation



Citation: Alani, O.A.; Ari, H.A.; Alani, S.O.; Offiong, N.-A.O.; Feng, W. Visible-Light-Driven Bio-Templated Magnetic Copper Oxide Composite for Heterogeneous Photo-Fenton Degradation of Tetracycline. *Water* **2021**, *13*, 1918. <https://doi.org/10.3390/w13141918>

Academic Editor: Chang Min Park

Received: 1 June 2021

Accepted: 26 June 2021

Published: 12 July 2021

Publisher's Note: MDPI stays neutral with regard to jurisdictional claims in published maps and institutional affiliations.



Copyright: © 2021 by the authors. Licensee MDPI, Basel, Switzerland. This article is an open access article distributed under the terms and conditions of the Creative Commons Attribution (CC BY) license (<https://creativecommons.org/licenses/by/4.0/>).

1. Introduction

The shortage of clean water supplies is the most pressing challenge causing widespread concern in the world today [1]. The world has been placed under a lot of pressure as several organic chemicals have been recognized as possible emergent contaminants in the environment. Antibiotics are one of the most common evolving contaminants as they are commonly utilized for the treatment of ailments in Man and animals [2]. Tetracyclines (TCs) are among the most extensively utilized antibiotics in human medicine, animal disease management, and agricultural dietary supplements owing to their broad spectrum of action, high quality, and low cost [2–4]. Unfortunately, TC is weakly metabolized in the digestive tract, and about 70% of it is excreted by urine and feces leading to increasing TC contamination of water systems and posing a severe threat to ecosystems [5–8]. As

a result, TC is commonly found in soil, surface water, and drinkable water, therefore, needs to be removed due to its tendency to cause human allergies and microbial resistance genes [9–12].

Among the various methods employed for treating contaminated water, advanced oxidation processes (AOPs) are a potential and efficient approach for degrading non-biodegradable organic pollutants in industrial wastewater [2,7,8,13,14]. The heterogeneous Fenton process, a type of AOP, is being explored to address the traditional Fenton process's main drawbacks, such as the restricted pH range (2.8–3.5), the production of iron sludge, and the treatment of secondary pollution [15–19]. Despite the many benefits of the heterogeneous Fenton method over the traditional Fenton method, its commercial deployment in wastewater treatment has been limited, because of the decreased efficiency rates of degradation and the high utilization rates of H₂O₂. Therefore, significant attempts to boost the heterogeneous Fenton process effectiveness are tailored through catalyst designing and modification is recently receiving a lot of attention [20–22].

According to some recent research, photo-excited electrons generated by semiconducting materials have been identified to enhance the degradation efficiency of the heterogeneous Fenton process [9,23–25]. Due to their large bandgap, some metal oxides, like TiO₂ and ZnO that have been employed to enhance the heterogeneous Fenton process, can be excited only by ultraviolet radiation. Ultra-violet light energy accounts for just around 4% of the whole solar spectrum, resulting in poor solar energy utilization efficiency. To maximize solar energy utilization, metal oxides that can be activated in the visible light part of the solar spectrum are attracting a lot of attention [26–29].

CuO is a promising option for the production of the visible-light-driven catalyst since it is a p-type semiconductor with a low bandgap of 1.7 eV and is suitable for capturing solar light energy [30–34]. Other distinguishing properties of CuO such as high abundance, relatively inexpensive, low toxicity, straightforward multiple ways of preparation, and its environmentally benign character have made the metal oxide appropriate for use in a wide range of fields including solar energy, semiconductors, lithium-ion batteries, memory devices, and field-effect transistors, and photocatalysts [28,35–37]. Therefore, we are convinced that binary complexes of Fe-CuO like heterojunction architectures can boost heterogeneous Fenton activity because the photoinduced electron produced by the metal oxides will allow for a long-term Fe³⁺/Fe²⁺ cycling reaction and enhance efficient utilization of visible light.

Non-metals such as sulfur, carbon, nitrogen, and fluorine have been successfully employed to improve the photocatalytic activity of mixed oxides for degrading contaminants from wastewater [38–41]. Among the non-metals, carbon materials have gained wide applications as support-based materials for semiconductors. In addition to acting as a support or adsorbent, some studies have shown that carbon can function as a sensitizer, transferring electrons to the metal oxides and promoting the creation of highly reactive radicals, thus improving semiconductor photocatalytic activity for specific reactions. This could explain why some semiconductors' photocatalytic activity has been extended into the visible light range [26,27,42–44]. Among the various carbon material sources, corn stalk biomass has attracted considerable interest because it is an agricultural waste, cheap, and containing high amounts of organic matter that can be tailored to the desired end-use [27,45]. The design of cost-effective, highly efficient, and reusable visible-light-driven heterogeneous Fenton-like catalysts remained a major concern to date.

In this work, a two-step procedure of bio-template and hydrothermal synthesis was used to create a visible-light-driven magnetic copper oxide (Fe₃O₄/CuO/C) composite. The biomass source is a corn stalk on which CuO and polyhedral Fe₃O₄ nanoparticles were grown in-situ. The interfacial interaction of the prepared composite enhances the cycle efficiency of Fe³⁺/Fe²⁺ in the heterogeneous photo-Fenton reaction while also addressing the issue of photo-generated electron and hole recombination. TC was selected as the target pollutants for degradation by the heterogeneous photo-Fenton system irradiated by visible light. Influencing factors including the initial concentration of H₂O₂, initial

pH value, catalyst dosage, and initial TC concentration were investigated. The prepared catalyst performed excellently in degrading TC between the pH range of 3–9 and exhibit remarkable stability after 5 cycles of consecutive reuse. A plausible reaction mechanism was proposed.

2. Materials and Methods

2.1. Materials

Copper sulfate pentahydrate ($\text{CuSO}_4 \cdot 5\text{H}_2\text{O}$), ferrous sulfate ($\text{FeSO}_4 \cdot 7\text{H}_2\text{O}$), sodium thiosulfate pentahydrate ($\text{Na}_2\text{S}_2\text{O}_3 \cdot 5\text{H}_2\text{O}$), sulfuric acid, formic acid, p-benzoquinone (BQ), silver nitrate (AgNO_3), tert-butyl alcohol (TBA), and ethanol were purchased from Sinopharm Chemical Reagent Co. Ltd. (Shanghai, China). Hydrogen peroxide 30% (H_2O_2), sodium hydroxide (NaOH) were obtained from Beijing Chemical Works (Beijing, China). Tetracycline hydrochloride ($\text{C}_{22}\text{H}_{24}\text{N}_2\text{O}_8\text{HCl}$) was obtained from Genview Scientific Inc (Tampa, FL, USA). All of the chemicals were analytical grade and were not purified any further. All of the solutions were made with deionized water.

2.2. Synthesis of Bio-Templated CuO

Cornstalk was treated with 5% weak aqueous NH_3 solution at 80 °C for 3 h to remove lignin, hemicellulose, and other inherent impurities. The treated cornstalk was filtered and rinsed with distilled water several times before being dried at 60 °C for 24 h. A specific amount of the treated cornstalk was steeped in a solution of $\text{CuSO}_4 \cdot 5\text{H}_2\text{O}$ (80 mM) followed by the addition of NaOH (10 mM) and kept at 60 °C for 24 h. The cornstalk-loaded CuO was washed several times with distilled water after 24 h and then dried at 60 °C. The dried prepared cornstalk-loaded CuO was calcinated at 550 °C for 5 h in a tube furnace heating at a rate of 1 °C/min under a nitrogen atmosphere. The resultant product of this stage is a bio-templated copper oxide (CuO/C).

2.3. Synthesis of Bio-Templated Magnetic Copper Oxide ($\text{Fe}_3\text{O}_4/\text{CuO}/\text{C}$)

The hydrothermal procedure was employed for the preparation of $\text{Fe}_3\text{O}_4/\text{CuO}/\text{C}$. In brief, a suitable amount of the prepared bio-templated copper oxide, $\text{FeSO}_4 \cdot 7\text{H}_2\text{O}$ (5.0 mM), and $\text{Na}_2\text{S}_2\text{O}_3 \cdot 5\text{H}_2\text{O}$ (5.0 mM) were dispersed in 30 mL of distilled water. The mixture was agitated for 10 min, before adding NaOH (10 mM) solution in drops. The mixture was then agitated for a further 5 min, before being placed into a 50 mL Teflon-lined autoclave. After sealing the Teflon-line autoclave, the temperature was raised to 140 °C for 12 h before being allowed to cool naturally to ambient temperature. After washing with ethanol and distilled water, the resultant residue was dried at 60 °C. The composition of the prepared bio-templated copper oxide (CuO/C) and $\text{FeSO}_4 \cdot 7\text{H}_2\text{O}$ were varied in the ratio of 1:1, 2:1, 1:2, and 1:3, respectively. The procedure was repeated for the synthesis of Fe_3O_4 without the prepared bio-templated copper oxide.

2.4. Characterization

Analyzes were carried out using an XL-30 ESEM FEG scanning electron microscope and energy dispersive spectrometry (EDS). The crystal phase of all the composites was studied using X-ray diffraction (XRD) on a Rigaku D/Max 2550 diffract meter (Rigaku Corporation, Tokyo, Japan) with a Cu-k radiation source ($k = 1.54056$) at a 10 °C min^{-1} scan rate. The composite's elemental analysis was undertaken by X-ray photoelectron spectroscopy (XPS, ESCA LAB 220-XL, Al $K\alpha$ radiation). Thermogravimetric analysis (TGA) of the samples was undertaken in air on an SDT Q600 thermal gravimetric analyzer (TA Instruments, USA) from room temperature to 800 °C at a 10 °C min^{-1} ramping rate. For the identification of functional groups in the region of 4000–400 cm^{-1} , Fourier transform infrared (FTIR) spectroscopy (Nexus 670, Nicolet, USA) was used. The prepared catalyst's electrochemical properties were determined on an electrical workstation with a three-electrode cell system (CHI660E Shanghai Chenhua Instrument Co., Ltd., Shanghai, China). The Ag/AgCl served as the reference electrode, Pt wire served as the counter electrode,

and Fe₃O₄ and Fe₃O₄/CuO/C catalyst coated on flourine-tine oxide (FTO) conductive glass served as the working electrode. The electrochemical impedance spectroscopy was recorded at an open circuit potential of 0.1 M K₄Fe(CN)₆ electrolyte solution at a frequency range of 1 × 10⁵ to 10² Hz and an amplitude of 5 mA to analyze the conductivity of the prepared working electrode. A Lakeshore 735 vibrating sample magnetometer (VSM) was used to evaluate the magnetic properties of the prepared catalyst at ambient temperature.

2.5. Catalytic Performance of Prepared Catalyst on Tetracycline (TC)

The catalytic performance of the prepared Fe₃O₄/CuO/C catalyst was assessed by degrading an aqueous TC solution under visible light irradiation (λ = 420 nm). By putting 0.3 g of Fe₃O₄/CuO/C into 100 mL of TC aqueous solution (50 mg/L) in a glass beaker with continuous agitation, the reactions were carried out. To achieve a TC-catalyst adsorption-desorption equilibrium, the aqueous suspension was agitated for 30 min in the dark. The catalytic heterogeneous photo-Fenton reaction was initiated by adding a specified amount of H₂O₂ to the reaction vessel while simultaneously putting on a 100W Xe lamp (λ = 420 nm) for visible light irradiation. Approximately 5 mL aliquots were collected at a set interval and filtered immediately with 0.45 μm membrane filters. An ultraviolet-visible (UV-Vis) spectrophotometer was used to determine the concentration of residue TC by measuring its absorbance at 357 nm (SOPTOP 757). After the reaction, the catalyst was retrieved using an external magnetic field, rinsed with deionized water, and dried for 2 h at 60 °C before being recycled. Equation (1) was used to calculate the rate of TC degradation in each procedure using the synthesized Fe₃O₄/CuO/C catalyst. The experiments were carried out in triplicate, with the average results being presented. We retested the efficiency of the prepared Fe₃O₄/CuO/C catalyst for five consecutive cycles to assess its recyclability and stability.

$$\text{Percent degradation} = \frac{(C_0 - C_t)}{C_0} \times 100 \quad (1)$$

where C_0 was the initial TC concentration at time $t = 0$, and C_t was the concentration of TC at time t .

3. Results and Discussion

3.1. Results of Characterization

3.1.1. X-ray Diffraction (XRD) Analysis

The crystalline phases of the synthesized CuO/C, Fe₃O₄, and Fe₃O₄/CuO/C were confirmed using X-ray diffraction analysis, and the results are presented in Figure 1. For CuO/C (Figure 1a), the diffraction peaks were observed at $2\theta = 32.5$ (110), 35.4 (-111), 38.708 (111), 46.3 (-112), 53.5 (020), 58.3 (202), 61.5 (-113), 66.2 (-311), 68.123 (220) corresponding to the plane of monolithic CuO structure, these values matching to the standard Joint Committee on Powder Diffraction Standards card number (JCPDS No. 48-1548) [28,30]. The diffraction peaks of Fe₃O₄ were observed at $2\theta = 30.1$ (220), 35.5 (311), 43.1 (400), 53.2 (422), 57.0 (511) and 62 (440) corresponding to JCPDS card number (JCPDS No. 75-0033) [46]. The diffraction peaks of CuO and Fe₃O₄ are well indexed in the Fe₃O₄/CuO/C diffraction pattern corresponding to JCPDS card number (JCPDS No. 75-1517); the majority of the peaks are associated with the monolithic structure of CuO and magnetite Fe₃O₄, which confirms the successful synthesis of Fe₃O₄/CuO/C composite [47]. In addition, there are no impure peaks, indicating that the cornstalk's natural carbon components have been destroyed. In all the Fe₃O₄/CuO/C ratios (Figure 1b), the peak at 35.5° can be matched to both the (-111) plane in the CuO phase and the (311) plane in the Fe₃O₄ phase, signifying the existence of the Fe₃O₄/CuO/C heterojunctions [48]. The diffraction peak of Cu in the Fe₃O₄/CuO/C composite spectrum is similarly stronger compared to that of Fe, implying that metallic copper possesses a high crystallinity [34,37].

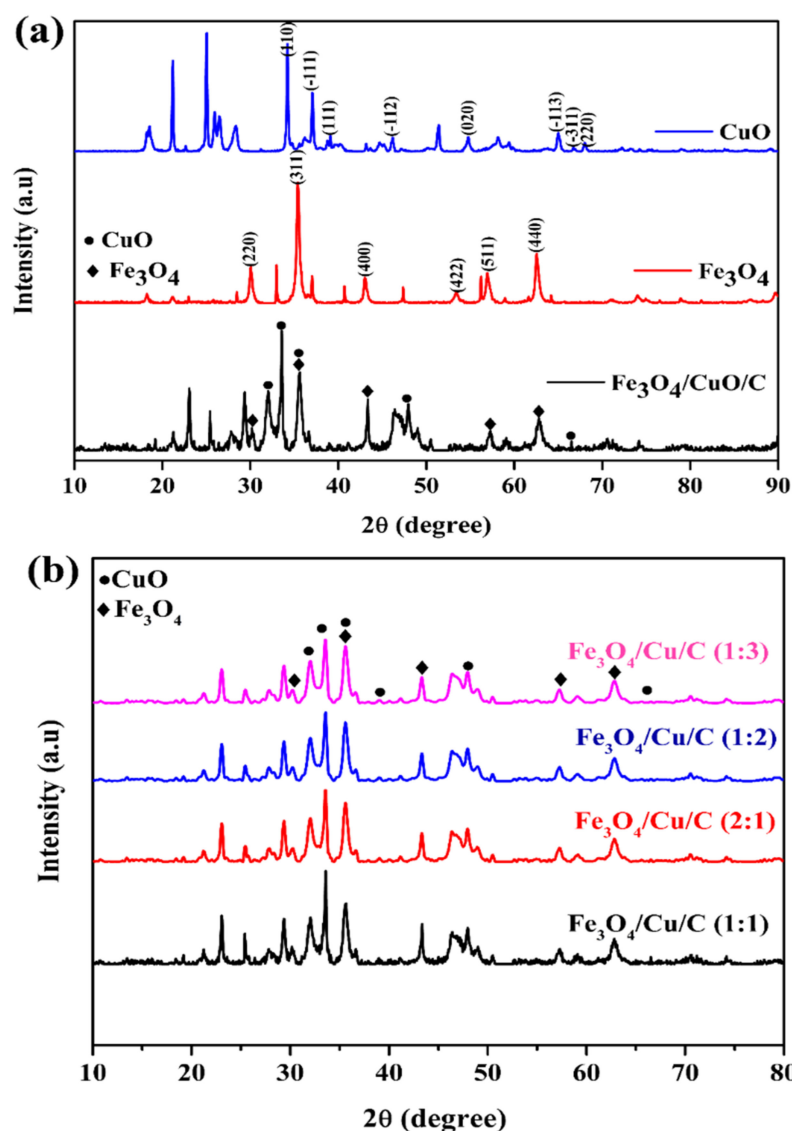


Figure 1. X-ray diffraction (XRD) patterns of CuO, Fe₃O₄, and Fe₃O₄/CuO/C (a) XRD patterns of Fe₃O₄/CuO/C with different ratios of CuO and Fe₃O₄ (b).

3.1.2. Fourier Transform Infrared (FTIR) Spectroscopy Analysis

The FTIR spectrum of Fe₃O₄, CuO/C, and Fe₃O₄/CuO/C (2:1) are shown in Figure 2. Three essential bands of interest in the FTIR spectrum of Fe₃O₄ nanoparticles are 585, 1637, and 3413.73 cm⁻¹, corresponding to Fe–O bonds in the crystal lattice of Fe₃O₄, C–H, and O–H bonds, respectively. The C–H and O–H bonds' appearance in this spectral is probably due to the use of ethanol and water during synthesis; this observation was corroborated and reported by previous researchers [49,50]. The FTIR spectrum of CuO/C has a sharp band at around 681 cm⁻¹, which is associated mostly with Cu–O stretching mode, 1619 cm⁻¹, related to the C–H band, confirming carbon's presence serving as the organic skeleton supporting the CuO nanoparticles [51,52]. The broadband at around 3313.31 cm⁻¹ is due to stretching O–H molecules present in the CuO/C [53]. The spectrum of Fe₃O₄/CuO/C consists of the prominent bands of 581, 675, 1631, and 3500–3100 cm⁻¹ corresponding to Fe–O of Fe₃O₄, Cu–O of CuO, C–H of bio-templated CuO, and O–H of inherent and adsorbed water molecules, respectively [47,53]. Thus, the formation of Fe₃O₄/CuO/C composite is also confirmed from the FTIR analysis.

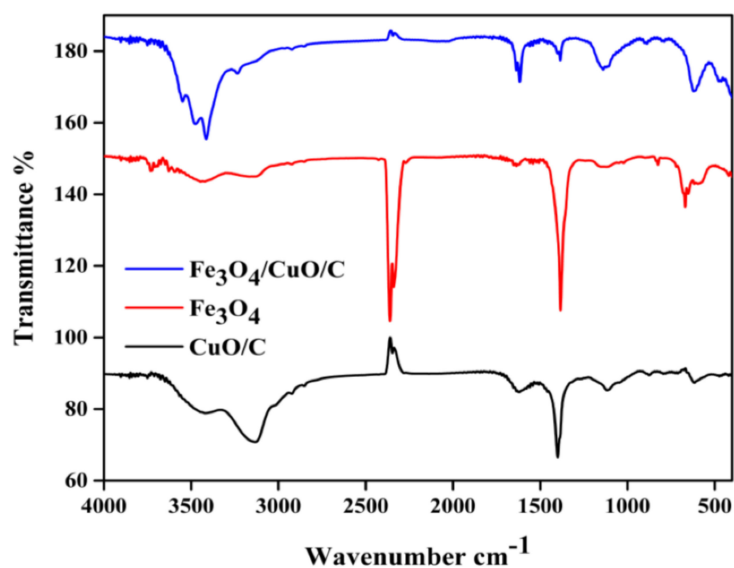


Figure 2. Fourier transform infrared (FTIR) analysis of CuO/C, Fe₃O₄, and Fe₃O₄/CuO/C.

3.1.3. Thermogravimetric (TG) Analysis

To determine the presence of carbon in the prepared Fe₃O₄/CuO/C catalyst, TG analysis was carried out in the air. The weight loss between room temperature and 280 °C is attributable to the elimination of absorbed water in Figure 3. The weight gain from around 280 and 335 °C is attributable to the oxidation of both CuO and Fe₃O₄ [34,37]. After 335 °C, the weight loss may be attributable to carbon oxidation, confirming the existence of carbon in the prepared catalyst matrix [54].

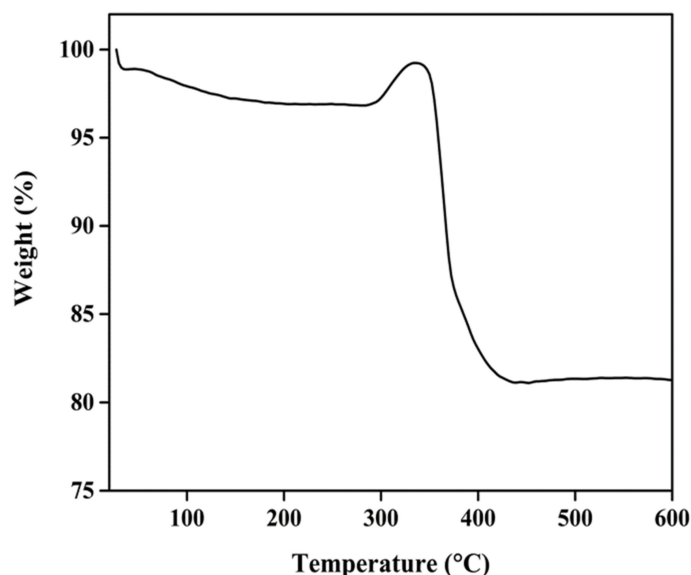


Figure 3. Thermogravimetric (TG) curve of Fe₃O₄/CuO/C.

3.1.4. Field Emission-Scanning Electron Microscopy (FE-SEM) Analysis

The morphology of the catalyst Fe₃O₄/CuO/C was examined by field emission-scanning electron microscopy (FE-SEM). Figure 4a shows that the CuO particles are dense and closely packed compare to CuO/C (Figure 4b) which has been loosened because of the presence of carbon template; while Fe₃O₄ (Figure 4c) are agglomerated particles with an irregular shape. Figure 4d, Fe₃O₄/CuO/C (2:1), shows that the prepared catalyst retains the cornstalk hierarchical porous organic structure after the template was removed.

The template creates a porous structure that favours particle interconnectivity, prevents photo-induced electron/hole recombination, and enhances TC molecules' adsorption.

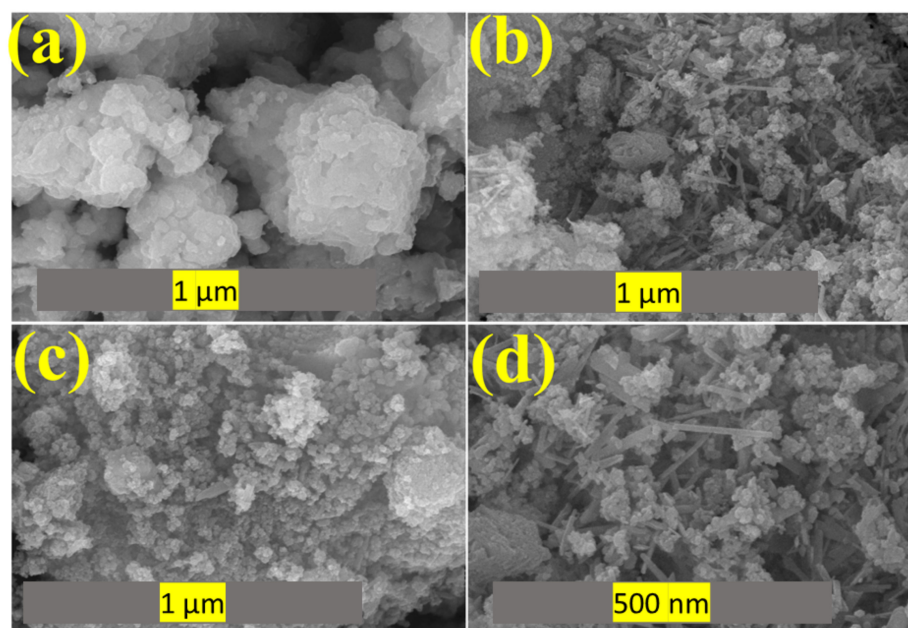


Figure 4. Scanning electron microscopy (SEM) image of CuO (a) CuO/C (b) Fe₃O₄ (c) Fe₃O₄/CuO/C (d).

3.1.5. Energy-Dispersive Spectrometry (EDS) Analysis

The EDS analysis confirms the elemental composition of the prepared Fe₃O₄/CuO/C catalyst. Figure 5 shows that Cu, Fe, C, and O are the main constituents of Fe₃O₄/CuO/C with different weight percentages of 11.68%, 19.51%, 42.24%, and 23.03%, respectively. This confirms the successful synthesis of the Fe₃O₄/CuO/C composite.

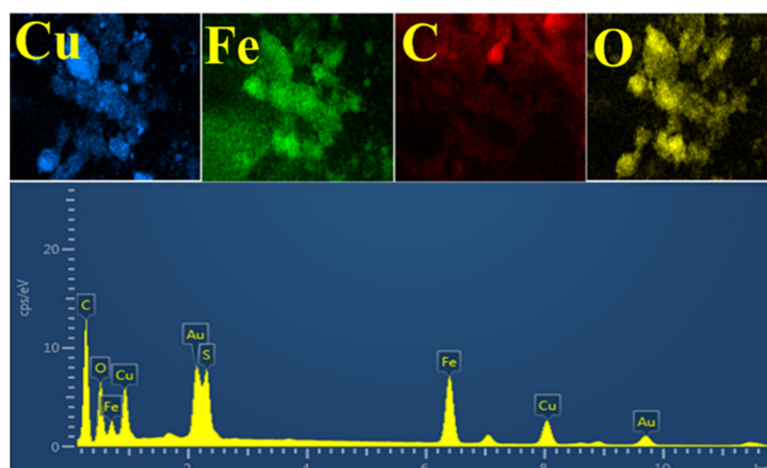


Figure 5. Energy-dispersive spectrometry (EDS) elemental mapping.

3.1.6. X-ray Photoelectron Spectroscopy (XPS) Analysis

The chemical composition of the prepared Fe₃O₄/CuO/C catalysts and electronic configurations were also determined by X-ray photoelectron spectroscopy (XPS). The wide scan spectral of CuO/C, Fe₃O₄, and Fe₃O₄/CuO/C is displayed in Figure 6a. At the same time, Figure 6b–d is the deconvoluted spectral of Cu 2p, Fe 2p, and O1s respectively of the prepared Fe₃O₄/CuO/C. The XPS spectral of Cu 2p was deconvoluted into four different binding energies of 933.5, 942, 953.6, and 962.2 eV (Figure 6b). The high-resolution peaks appearing at 933.7 and 953.4 eV assigned to Cu 2p_{3/2} and Cu 2p_{1/2} reveal that the oxidation

state of Cu is Cu^{2+} in the prepared $\text{Fe}_3\text{O}_4/\text{CuO}/\text{C}$ catalyst [35,55]. Also, two satellite peaks were observed at 942 and 962.2 eV, which correspond to the d9 configuration of Cu^{2+} confirming the existence of CuO; this observation was similar to what has been reported previously [28,56]. Figure 6c shows a typical Fe 2p spectrum with two notable peaks at 711.2 and 724.5 eV, which correspond to the Fe 2p_{3/2} and Fe 2p_{1/2} spin-orbit split doublets, respectively; the results are consistent with earlier studies [34,57]. Moreover, when we compared the position of Cu 2p (Figure 6b) and Fe 2p (Figure 6c) in their pure and composite form, there was a redshift in binding energy, which really is advantageous for light excitation. Furthermore, the XPS deconvoluted spectrum of O1s with peaks at 533.3, 531.1, and 530.4 eV (Figure 6d) are the binding energy of lattice and adsorbed oxygen elements respectively [28,34,56]. The binding energies of the two peaks in the deconvoluted C1s XPS spectra of $\text{Fe}_3\text{O}_4/\text{CuO}/\text{C}$ are 288.7 and 284.1 eV, respectively, corresponding to C–O, and C–C, with the conspicuous peak at 284.8 eV typically attributable to elemental carbon [58]. This means that some quantity of carbon from cornstalk has been doped into the CuO lattice, making it charge transfer sensitive when exposed to light [59,60]. Finally, the standard reference carbon may be assigned to the C 1s peak in the survey XPS spectra of Fe_3O_4 [61].

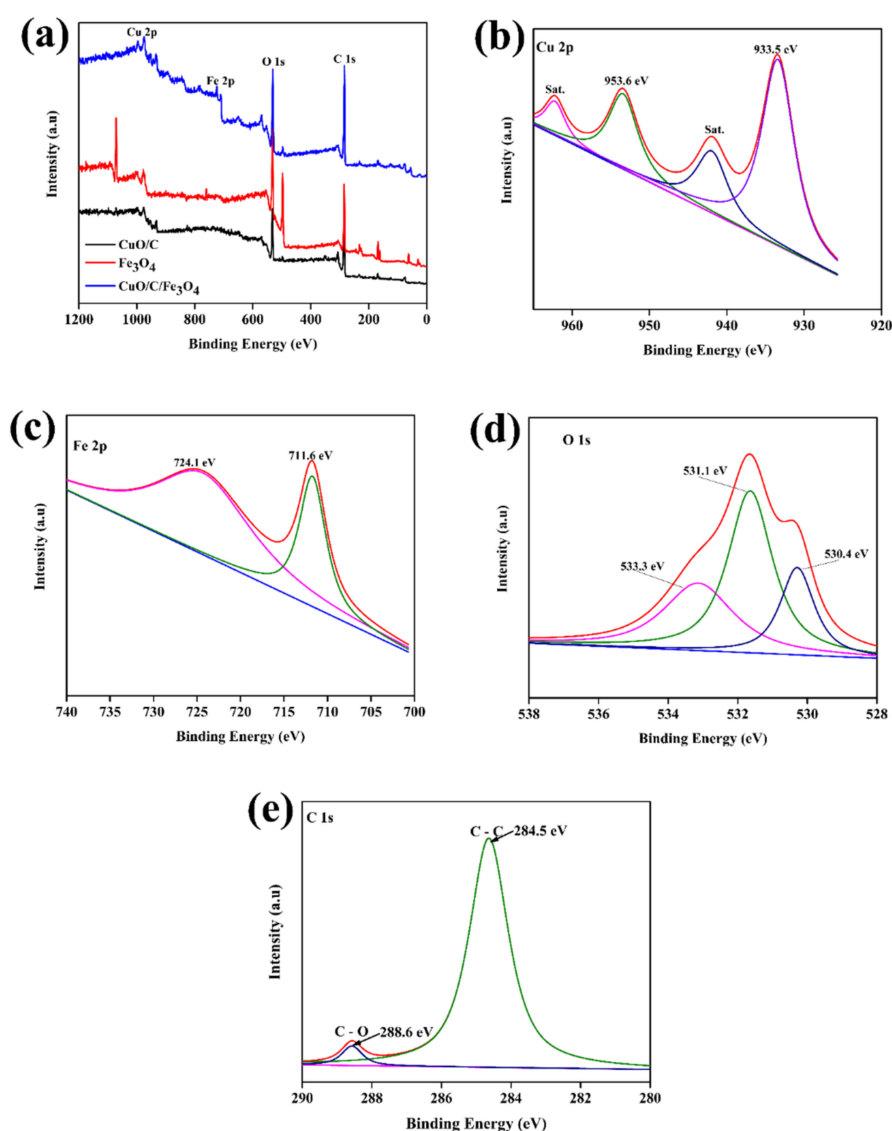


Figure 6. X-ray photoelectron spectroscopy (XPS) wide scan of CuO/C, Fe_3O_4 , and $\text{Fe}_3\text{O}_4/\text{CuO}/\text{C}$ (a), deconvoluted XPS spectral of $\text{Fe}_3\text{O}_4/\text{CuO}/\text{C}$ (b–e).

3.1.7. Electrochemical Impedance Spectroscopy (EIS) Analysis

The electrochemical characteristics of the produced catalyst were measured using electrochemical impedance spectroscopy (EIS). A semicircle in the high-frequency region and a sloping line in the low-frequency region make up the Nyquist plot of the constructed electrodes (Figure 7). Compared to Fe_3O_4 , the arc radius of the $\text{Fe}_3\text{O}_4/\text{CuO}/\text{C}$ electrode has a low resistivity, implying that the prepared $\text{Fe}_3\text{O}_4/\text{CuO}/\text{C}$ catalyst has a reduced electrochemical resistance, translating to a faster rate of electron transfer from Fe^{3+} to Fe^{2+} , thus contributing to a reduction in the associated energy consumption rate compared to Fe_3O_4 , leading to an improved reaction process for the heterogeneous photo Fenton catalyst.

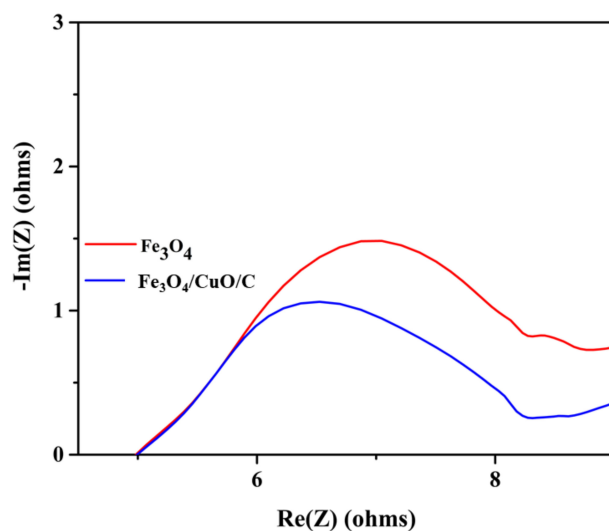


Figure 7. Electrical impedance spectroscopy (EIS) $\text{Fe}_3\text{O}_4/\text{CuO}/\text{C}$, and Fe_3O_4 .

3.1.8. Magnetism Study

Figure 8 shows the Fe_3O_4 and $\text{Fe}_3\text{O}_4/\text{CuO}/\text{C}$ hysteresis loops studied at 300 K by vibrating sample magnetometer (VSM). The pure Fe_3O_4 's saturation magnetization (M_s) value is approx. 48.7 emu/g, while the composite of $\text{Fe}_3\text{O}_4/\text{CuO}/\text{C}$ is approx. 33.2 emu/g, suggesting that the prepared catalyst is superparamagnetic. The reduction in magnetic properties could be attributed to the presence of non-magnetic bio-templated CuO [20,25]. Following separation and manipulation by an external magnetic field, $\text{Fe}_3\text{O}_4/\text{CuO}/\text{C}$ can also be easily re-dispersed for reuse, as seen in the inset of Figure 8. As a result, it can improve the $\text{Fe}_3\text{O}_4/\text{CuO}/\text{C}$ catalyst's separation, recovery, and reusability.

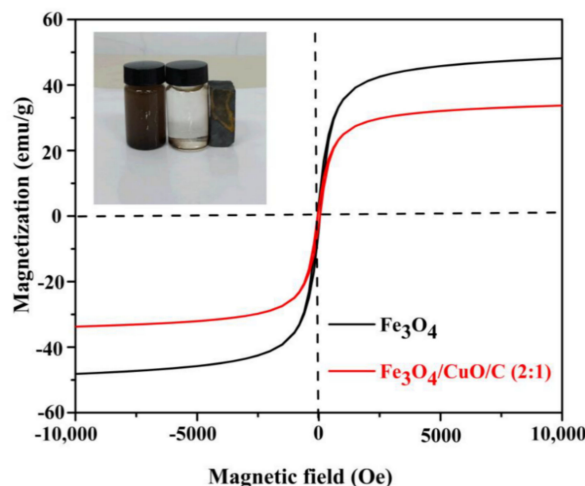


Figure 8. Magnetic hysteresis loops of Fe_3O_4 and $\text{Fe}_3\text{O}_4/\text{CuO}/\text{C}$ (2:1) nanoparticles at 300 K.

3.2. Evaluation of Catalytic Performance on TC Degradation

3.2.1. The Catalytic Activities of Different Catalyst Systems

Evaluation of the synergistic effect of the synthesized catalysts on TC degradation was performed under visible light irradiation at pH 7 for 60 min and at a temperature of 25 °C. The result indicated that visible light does not have any significant impact on the degradation of the TC (Figure 9a). The combined effect of visible light-H₂O₂ achieved 11.5% TC removal which is due to the slight photolysis of H₂O₂ under the influence of solar light as the reaction vessel was insulated from the influence of solar light previous researchers have reported the instability of H₂O₂ under the solar spectrum [62,63], while visible light-Fe₃O₄/H₂O₂ (photo Fenton) achieved 76.3% degradation, and the combined impact of visible light-CuO (photocatalyst) could achieve 57% TC removal (Figure 9a). TC degradation with the visible light/Fe₃O₄/CuO/C/H₂O₂ (heterogeneous photo Fenton) system achieved 96.1% TC removal. When the photo-Fenton activity of Fe₃O₄ was compared to that of Fe₃O₄/CuO/C, the result showed that the performance of the latter was better than the former by 18.8% (Figure 9a). This result suggests that the interface binary complex of Fe₃O₄/CuO/C heterojunction contributed significantly to the heterogeneous photo-Fenton reaction. Therefore, we infer that the Fe₃O₄/CuO/C heterojunction interfaces significantly influence the photo-Fenton reaction using Fe₃O₄/CuO/C as the catalyst, which agrees with what has been previously reported [8,20]. From Figure 9b, the results show that the removal percent of TC with visible light/Fe₃O₄/CuO/C-H₂O₂ (2:1) was better compared to visible light/Fe₃O₄/CuO/C-H₂O₂ 1:1, visible light-Fe₃O₄/CuO/C-H₂O₂ (1:2), and visible light/Fe₃O₄/CuO/C-H₂O₂ (1:3) respectively. In the visible light/Fe₃O₄/CuO/C-H₂O₂ (2:1) system, the proportion of the heterojunction is optimal, compared to other ratios (1:1, 2:1, and 1:3). The result obtained emphasizes the importance of the adequacy of heterojunction to provide suitable interfaces for charge migration. Due to the outstanding performance of Fe₃O₄/CuO/C-H₂O₂ (2:1), it was adopted for further evaluation and characterization.

3.2.2. Influence of Catalyst Dosage

The influence of the initial dosage of catalyst on TC's degradation was evaluated as shown in Figure 10. According to Figure 10, only around 17% of the TC molecules could be adsorbed onto the Fe₃O₄/CuO/C catalyst surface during the adsorption-desorption stage, implying that the adsorption influence was inadequate. At the degradation stage, there was an increase in TC degradation efficiency as the dosage of the Fe₃O₄/CuO/C catalyst was increased from 0.1 to 0.3 g, but a slight decrease was observed as the dosage was further increased to 0.5 g. The possible reason for this decrease is that as the initial dosage of the catalyst exceeds 0.3 g, the particles of catalyst in the resultant aqueous suspension impede the light penetration and decrease the usage of light, resulting in decreased TC degradation efficiency. Other possible reasons are the agglomeration of catalyst particles and the excessive initial dosages of Fe₃O₄/CuO/C may act as a scavenger for the free radicals generated [64,65].

3.2.3. Influence of Initial Concentration of H₂O₂

The influence of the initial concentration of H₂O₂ was examined by using different concentrations of H₂O₂ in the Fe₃O₄/CuO/C-H₂O₂-visible light system. Figure 11 shows that increasing the H₂O₂ concentration from 15 to 30 mM improves the degradation efficiency somewhat. The efficiency of TC degradation decreases when the initial H₂O₂ concentration rises from 30 to 45 mM. The decrease in TC degradation efficiency with a rise in the concentration of H₂O₂ is attributable to the fact that H₂O₂ acts as a scavenger at a higher concentration, thereby decreasing the number of active radicals responsible for oxidizing TC molecules. Also at a higher concentration, H₂O₂ could generate HOO•, which has a lower oxidation potential than hydroxyl radical (•OH), thus inhibiting the efficiency of the process for TC degradation [66]. However, these results revealed that the initial concentration of H₂O₂ had minimal influence on the overall degradation rate because of the H₂O₂ low radical scavenging effect attributable to the low initial concentration of the

H_2O_2 that was used and the quick reaction between the TC molecule and the OH radicals generated. Therefore, an optimal initial concentration of H_2O_2 adequate in this work H_2O_2 is 30 mM.

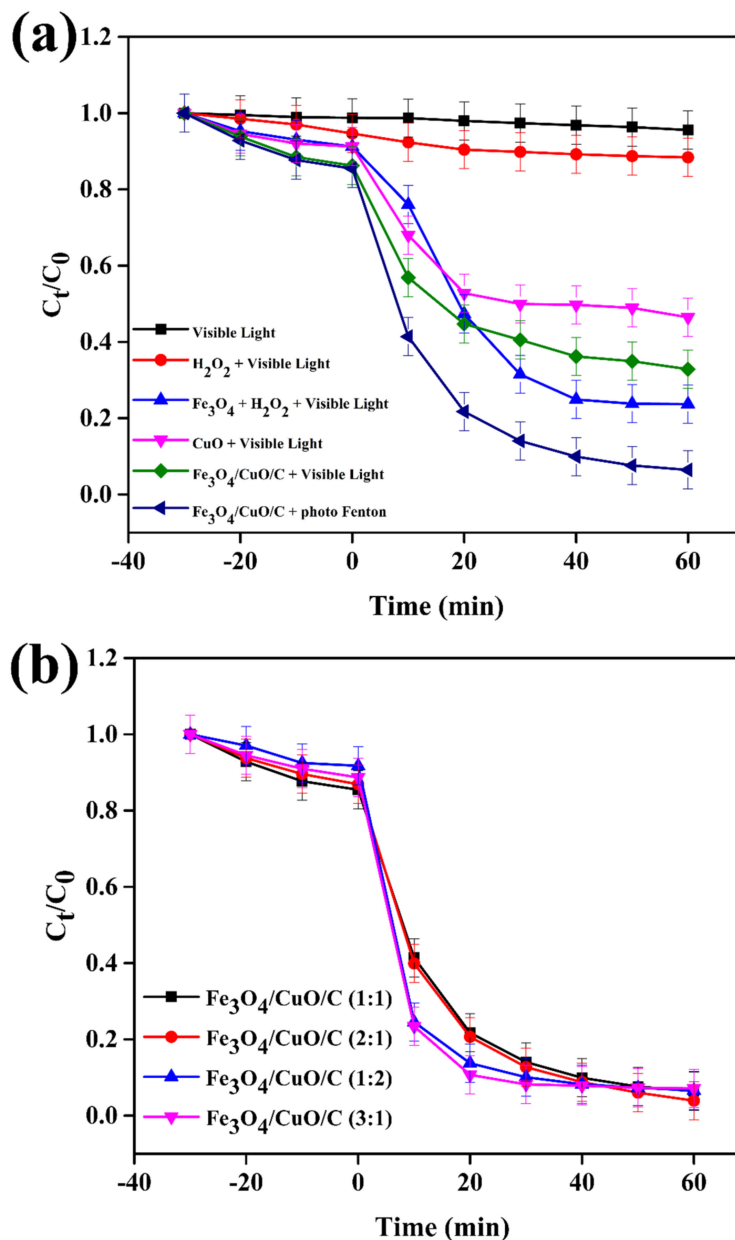


Figure 9. Degradation efficiency of tetracycline (TC) under different catalyst system (a) Comparison of photo-Fenton activity of $\text{Fe}_3\text{O}_4/\text{CuO}/\text{C}$ with different ratios of CuO/C and Fe_3O_4 (b) Experimental conditions: Except for the examined parameter, other parameters were fixed on initial pH = 7, TC concentration = 50 mg/L, catalyst mass = 0.3 g, H_2O_2 concentration = 30 mM, time = 60 min, temperature = 25 °C.

3.2.4. Influence of Initial pH

In TC degradation, the influence of the initial pH value cannot be overlooked [2,67]. Figure 12 depicts the effect of the initial pH value on the efficiency of TC degradation in this study. The maximum degradation efficiency of 96.1% was achieved at pH 3 and 7 while at pH 9 the efficiency of degradation is 91.4% which is also high. The results show that $\text{Fe}_3\text{O}_4/\text{CuO}/\text{C}$ composites can function over a wide range of pH. This effectiveness may be attributed to the development of acidic intermediates, even if the starting pH is 7.0 or

9.0, the final pH is retained at an acidic medium under pH of 4.0 after 60 min [20,68]. As a result of this research, $\text{Fe}_3\text{O}_4/\text{CuO}/\text{C}$ composites catalyzing photo-Fenton TC degradation have outstanding photodegradation efficiency over a wide initial pH value range.

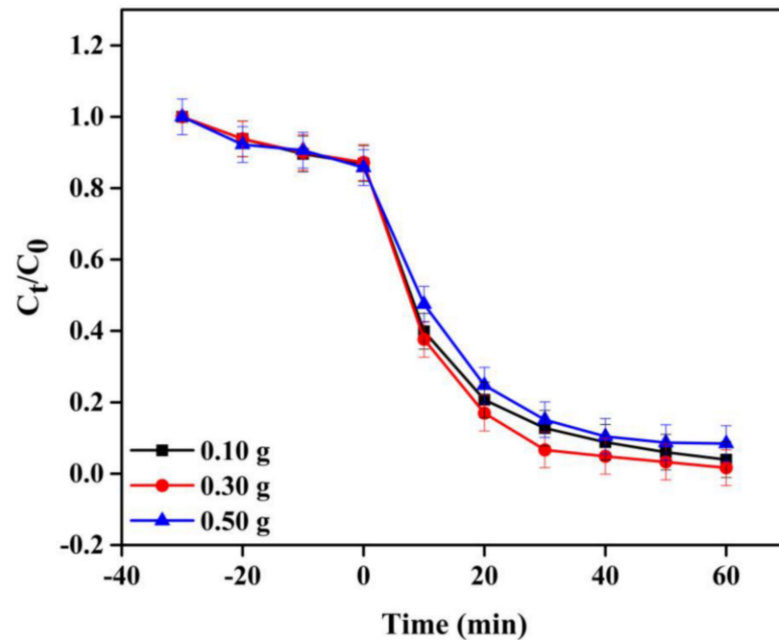


Figure 10. Influence of initial catalyst dosage. Experimental conditions: Except for the examined parameter, other parameters were fixed on initial pH = 7, TC concentration = 50 mg/L, H_2O_2 concentration = 30 mM, time = 60 min, temperature = 25 °C.

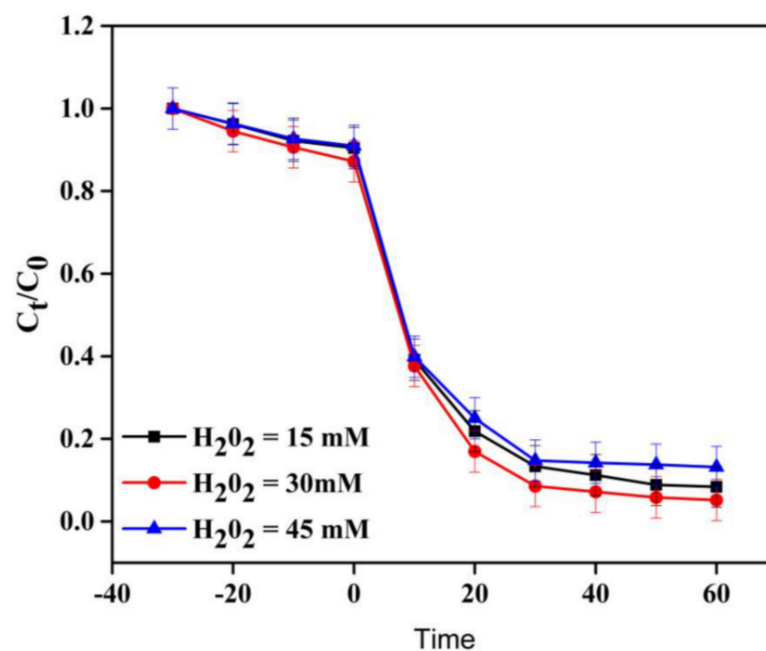


Figure 11. Influence of initial concentration of H_2O_2 . Except for the examined parameter, other parameters were fixed on TC concentration = 50 mg/L, catalyst mass = 0.3 g, time = 60 min, temperature = 25 °C.

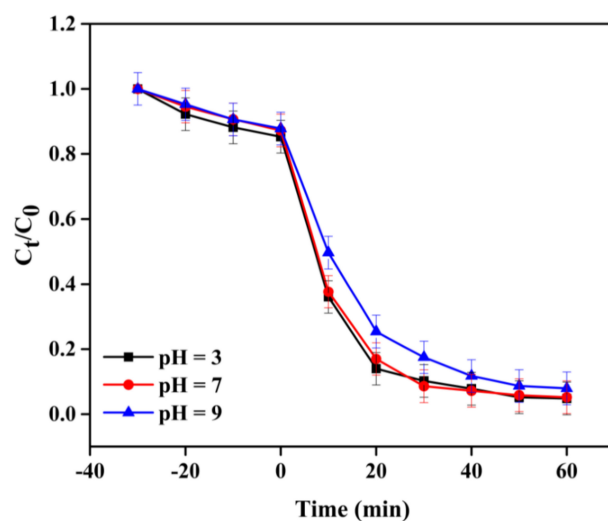


Figure 12. Influence of initial pH. Experimental conditions: Except for the examined parameter, other parameters TC concentration = 50 mg/L, catalyst mass = 0.3 g, H_2O_2 concentration = 30 mM, time = 60 min, temperature = 25 °C.

3.2.5. Influence of Initial TC Concentration

At a pH of 7 and a catalyst dosage of 0.3 g/L, the effects of initial TC concentration on photo-Fenton degradation were examined. The proportion of TC eliminated decreased from 96.1% to 83.3% when the starting concentration of TC was increased from 50 to 100 mg/L. (Figure 13). As the TC initial concentration increases from 50 to 75 and 100 mg/L, the number of TC molecules available for absorption on the $\text{Fe}_3\text{O}_4/\text{CuO}/\text{C}$ surface increases too, thus reducing the production of oxidant radicals and hence the photodegradation reaction. The decline in TC removal percentage could be due to the non-availability of active sites on the catalyst at higher TC concentrations, increasing the number of un-adsorbed TC molecules, because there was no commensurate rise in catalyst mass as TC concentration increased. An increased initial TC concentration reduces light irradiation penetration (screen effect), reduces $\bullet\text{OH}$ production; therefore, its photo-Fenton degradation efficiency is ultimately reduced.

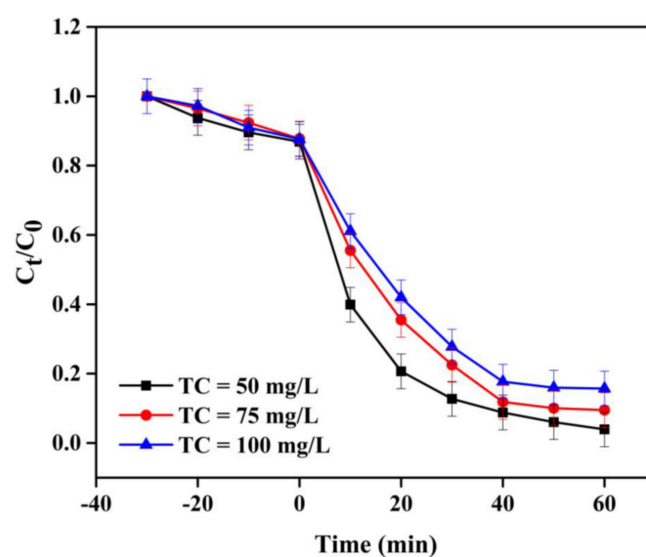


Figure 13. Influence of initial concentration of TC. Experimental conditions: Except for the examined parameter, other parameters catalyst mass = 0.3 g, H_2O_2 concentration = 30 mM, time = 60 min, temperature = 25 °C.

3.2.6. Kinetic Studies

Kinetic studies of TC degradation reactions exhibited a pseudo-first-order kinetic model concerning the irradiation time (Figure 14 and Table 1), with the rate of degradation given by Equation (2):

$$\ln \frac{C_t}{C_0} = -kt \quad (2)$$

where C_0 (mg/L) is the initial TC concentration at time $t = 0$, C_t (mg/L) is the TC concentration at time t , and k is the rate constant (min^{-1}).

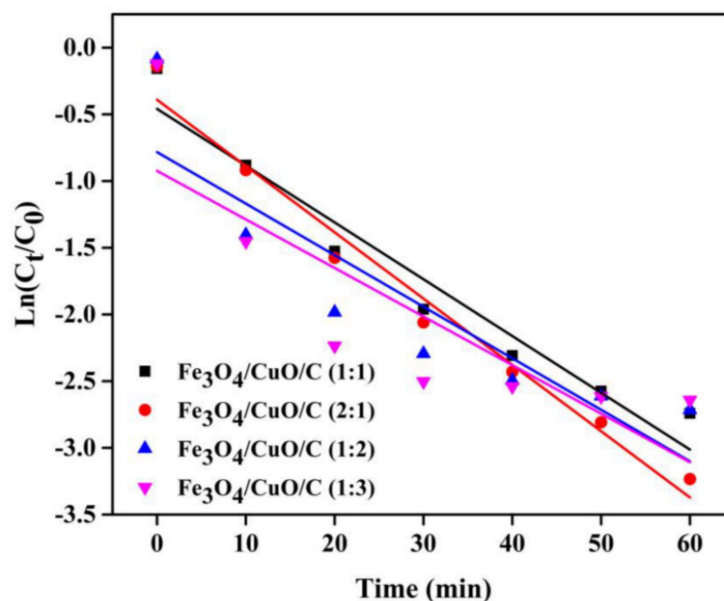


Figure 14. Plot of $\ln(C_t/C_0)$ against time. Experimental conditions: initial pH = 7, TC concentration = 50 mg/L, catalyst mass = 0.3 g, H_2O_2 concentration = 30 mM, time = 60 min, temperature = 25 °C.

Table 1. Rate constant values for TC degradation at different concentrations.

Rate Parameters	$\text{Fe}_3\text{O}_4/\text{CuO}/\text{C}$			
	(1:1)	(2:1)	(1:2)	(1:3)
Rate Constant k (min^{-1})	0.458	0.390	0.783	0.923
Initial reaction rate ($\text{mgL}^{-1} \text{min}^{-1}$)	0.042	0.049	0.038	0.036
Adjusted R-Square (R^2)	0.936	0.953	0.863	0.847

When the molar ratios of Fe_3O_4 and CuO/C were varied with irradiation time, a linear relationship for TC degradation was obtained (Figure 14). The slope and intercepts of these plots were used to calculate the rate constants, as indicated in Table 1. Table 2 shows an assessment of the catalytic activity of various photocatalysts utilized by various researchers for tetracycline degradation.

Table 2. The catalytic activity of various photocatalysts employed to degrade tetracycline was compared.

Catalyst	TC Concentration (mg/L)	Irradiation Time (min)	Percent of Degradation (%)	Number of Cycles	References
$\text{Fe}_3\text{O}_4/\text{CuO}/\text{C}$	50	60	99.1	5	Present work
$\text{TiO}_2/\text{Fe}_3\text{O}_4$	50	90	98	5	[20]
$\text{Fe}_3\text{O}_4@\text{void}/\text{TiO}_2$	40	06	≈ 100	5	[24]
Black- TiO_2	10	240	66.2	4	[69]
Schorl	100	600	95.2	5	[2]
MCB	100	3000	93.2	-	[5]
$\text{C}/\text{Fe}_3\text{O}_4/\text{Bi}_2\text{O}_3$	20	90	91	5	[44]

3.3. Influence of Different Radical Scavengers and Mechanism of Degradation

To figure out the main reactive species involved in this heterogeneous photo-Fenton process, a series of radical scavengers were introduced into the reaction vessel. The scavengers employed were TBA (5 mM) for $\bullet\text{OH}$, BQ (5 mM) for superoxide radical $\text{O}_2^{\bullet-}$ (5 mM) [29], AgNO_3 (5 mM) for photo-generated electrons (e^-), and formic acid for photo-generated holes (h^+) [25]. As shown in Figure 15, the photo-Fenton degradation of TC is partially suppressed after the addition of the radical scavengers. The photo-degradation reaction's suppression is in the following order $\text{BQ} > \text{TBA} > \text{AgNO}_3 > \text{Formic acid}$. Thus, it was deduced that $\bullet\text{OH}$, $\text{O}_2^{\bullet-}$, e^- , and h^+ oxidizing species were photo-generated onto the surface of $\text{Fe}_3\text{O}_4/\text{CuO}/\text{C}$. Therefore, in this heterogeneous photo-Fenton system of TC degradation, the $\text{O}_2^{\bullet-}$, $\bullet\text{OH}$, e^- , and h^+ play an essential role in the catalytic photo-Fenton reaction.

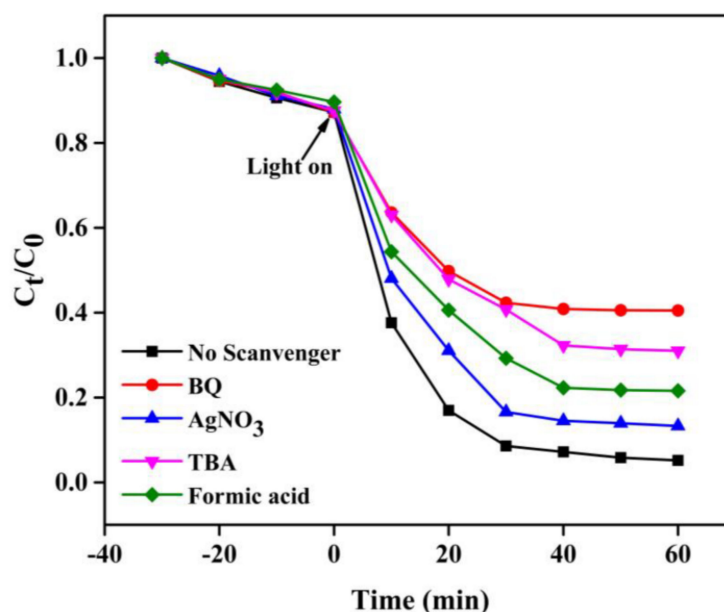


Figure 15. Influence of different radical scavengers. Experimental conditions: Except for the examined parameter, other parameters were fixed on initial pH = 7, catalyst mass = 0.3 g, H_2O_2 concentration = 30 mM, TC concentration = 50 mg/L, time = 60 min, temperature = 25 °C.

The plausible mechanism of photo-Fenton activity of the $\text{Fe}_3\text{O}_4/\text{CuO}/\text{C}$ in this combined system is based on the above results of radical scavenging as illustrated in Figure 15. Photogenerated electrons and holes are stimulated on the conduction band and valence band, respectively, when visible light is irradiated onto the surface of $\text{Fe}_3\text{O}_4/\text{CuO}/\text{C}$ (Equation (3)), and photolysis of H_2O_2 into OH occurs when visible light is irradiated onto the surface of $\text{Fe}_3\text{O}_4/\text{CuO}/\text{C}$. (Equation (4)). The photogenerated electrons at the conduction band combine with oxygen (O_2) to produce $\bullet\text{O}_2^-$ (Equation (5)) and promote regeneration of Fe^{2+} from Fe^{3+} (Equation (7)). Fe^{2+} combines with H_2O_2 to generate $\bullet\text{OH}$ (Equation (6)) while the adsorbed water is also photo catalytically oxidized into $\bullet\text{OH}$ by photogenerated holes in the valence band (Equation (8)). Therefore, we conclude that as it can be seen in Figure 16 the degradation of TC into CO_2 and H_2O (Equation (9)) is a result of the synergistic effect between $\bullet\text{OH}$ generated in Equations (4), (6) and (9) with $\text{O}_2^{\bullet-}$ in Equation (5). Compared with the homogeneous Fenton process, photo-induced electrons from the CuO surface enhances the $\text{Fe}^{3+}/\text{Fe}^{2+}$ cycle efficiency (Equation (6)). The Fe^{3+} release from the heterogeneous photo-Fenton process performs the role of an electron acceptor which hinders photo-generated electron-hole recombination, taking advantage of the well-suited interfacial interaction between $\text{Fe}_3\text{O}_4/\text{CuO}/\text{C}$ heterostructure. The carbon content in the prepared composite affords an enhanced microenvironment for trapping TC molecules from the aqueous solution. Thus, the heterojunction of $\text{Fe}_3\text{O}_4/\text{CuO}/\text{C}$ com-

posite improves the heterogeneous photo-Fenton performance process by enhancing the separation and use of photo-induced carriers.

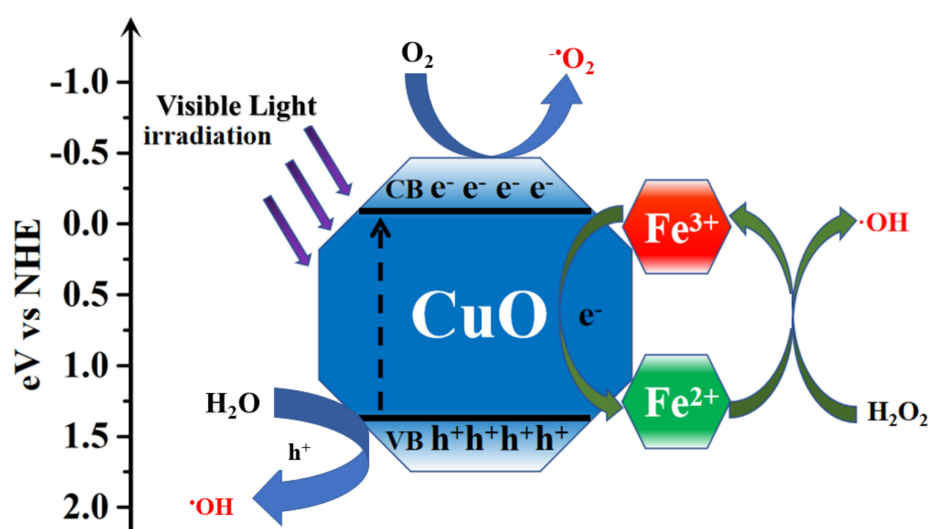
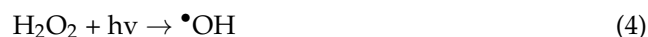


Figure 16. The proposed photo-Fenton-like mechanism for TC degradation in the presence of $\text{Fe}_3\text{O}_4/\text{CuO}/\text{C}$ composites is depicted schematically.

3.4. Mineralization Study for TC Degradation

After each treatment, the residual total organic carbon (TOC) content was measured to conduct the mineralization investigation for each of the catalyst systems. According to the results presented in Figure 17, the visible light process contained 100% residual TOC, the formation of $\bullet\text{OH}$ from photolysis of H_2O_2 has a TOC removal rate of 9%, visible light- $\text{Fe}_3\text{O}_4/\text{CuO}/\text{C}$ (photocatalyst) had a removal rate of 22%, while visible light- $\text{Fe}_3\text{O}_4-\text{H}_2\text{O}_2$ had a removal rate of 28% and visible light- $\text{CuO}/\text{C}/\text{Fe}_3\text{O}_4-\text{H}_2\text{O}_2$ had the highest TOC removal rate of 57%. The TOC removal rate of the visible light- $\text{CuO}/\text{C}/\text{Fe}_3\text{O}_4-\text{H}_2\text{O}_2$ was better than that of the homogeneous Fenton process from the results obtained in Figure 17.

3.5. Reusability and Stability Test

The recoverability, reusability, and stability of a catalyst is an essential consideration in adopting the catalyst for practical application. For reusability, the prepared $\text{Fe}_3\text{O}_4/\text{CuO}/\text{C}$ (2:1) composite was recycled five consecutive times, and there was not much loss of photocatalytic performance, as shown in Figure 18a, as 93.5% TC degradation was achieved after five runs. To evaluate the prepared catalyst's chemical stability, we characterized its residue by XRD, XPS, and FTIR analysis. The resulting Figure 18b–d, showed no discernible change in intensity in the XRD, XPS, and FTIR analysis before and after the five cycles of reuse of $\text{Fe}_3\text{O}_4/\text{CuO}/\text{C}$ composite. These results suggest that the prepared composite has good stability and can easily be adapted for water treatment and purification.

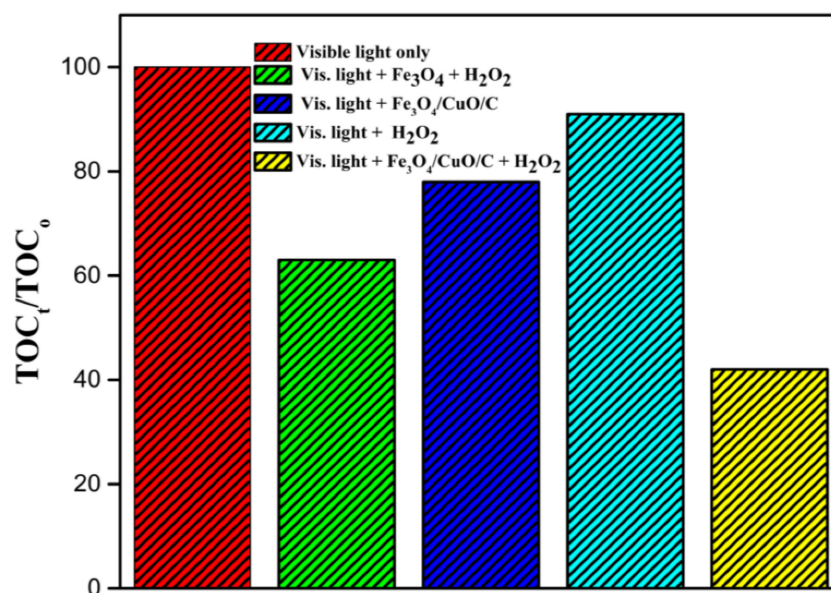


Figure 17. Mineralization of TC for the different catalyst systems.

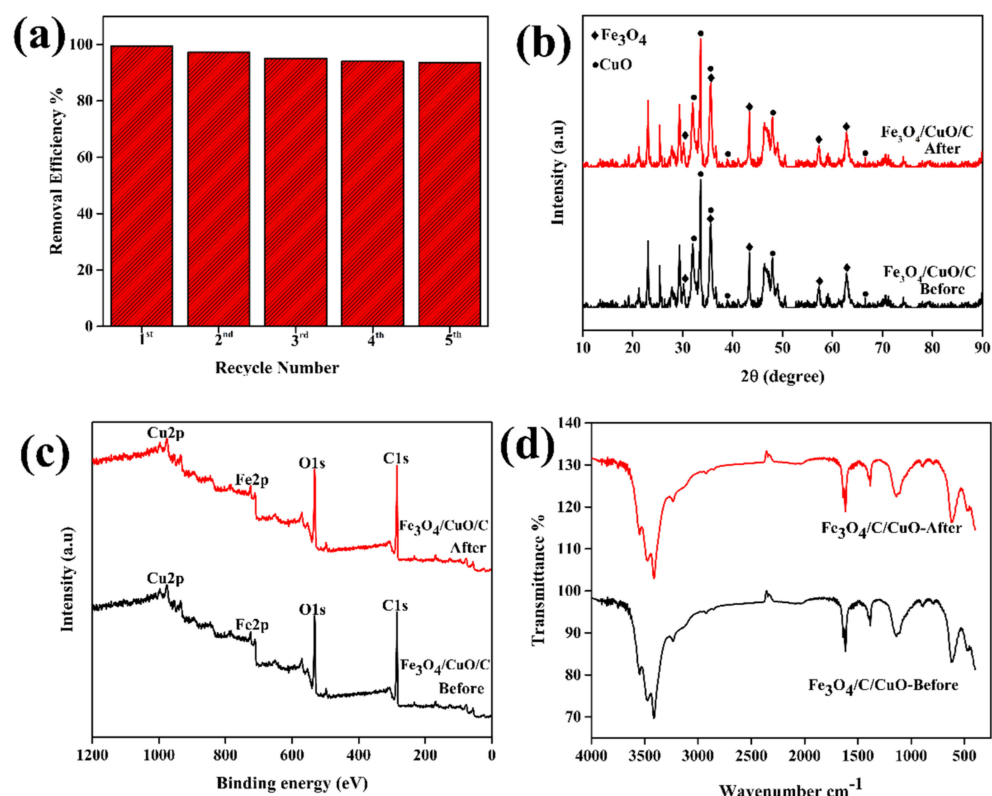


Figure 18. Reusability of Fe₃O₄/CuO/C for TC degradation (a), XRD pattern before and after degradation (b), XPS pattern before and after degradation (c), FTIR spectrum before and after degradation (d). Experimental conditions: initial pH = 7, TC concentration = 50 mg/L, catalyst mass = 0.3 g, H₂O₂ concentration = 30 mM, time = 60 min, temperature = 25 °C.

4. Conclusions

In conclusion, a visible-light-driven heterogeneous bio-templated magnetic copper oxide composite was created by a two-step of bio-templating and hydrothermal method. The produced Fe₃O₄/CuO/C catalyst composition was verified by XRD, SEM, EDS, FTIR, TGA, EIS, and VSM. The prepared catalyst performed excellently in photo-Fenton catalytic

degradation of tetracycline (TC) over a wide range of pH using visible light as an irradiation source. A microenvironment was generated by the presence of cornstark in the prepared catalyst composite to adsorb TC molecules, and the $\text{Fe}^{3+}/\text{Fe}^{2+}$ cycle efficiency was improved by interfacial interactions between Fe_3O_4 and CuO . Quite significantly, even after 5 cycles, the photo-Fenton activity remained high, indicating that the catalyst is highly stable and reusable. Using an external magnetic field, the catalyst was also easily recovered from the reaction medium. Because of its excellent performance in the visible region of the solar spectrum, $\text{Fe}_3\text{O}_4/\text{CuO}/\text{C}$ is a promising catalyst for heterogeneous photo-Fenton TC removal under visible light irradiation, maximizing the potential of solar energy and being more environmentally benign.

Author Contributions: Conceptualization, O.A.A. and W.F.; methodology, O.A.A. and H.A.A.; formal analysis, O.A.A.; investigation, O.A.A.; resources, W.F.; data curation, O.A.A.; data interpretation, O.A.A., H.A.A., N.-A.O.O.; writing—original draft preparation, O.A.A.; writing—review and editing, O.A.A., H.A.A., N.-A.O.O., S.O.A. and W.F.; supervision, W.F.; funding acquisition, W.F. All authors have read and agreed to the published version of the manuscript.

Funding: Financial supports from the Natural Science Foundation of China (Grant no. 61774073), the Open Project of State Key Laboratory of Inorganic Synthesis and Preparative Chemistry, Jilin University (No. 2016-25), and the Science and Technology Development Program of Jilin Province (No. 20170101086J) is also acknowledged.

Institutional Review Board Statement: Not applicable.

Informed Consent Statement: Not applicable.

Data Availability Statement: The data presented in this study are available on request from the corresponding author. The data are not publicly available due to privacy reasons.

Acknowledgments: The authors (Olushola Adewole Alani, Hadiza Abdullahi Ari, and Nnanake-Abasi O. Offiong) are grateful to the Petroleum Technology Development Fund (PTDF) Nigeria for foreign research scholarship.

Conflicts of Interest: The authors declare no conflict of interest.

References

1. Alani, O.A.; Ari, H.A.; Offiong, N.-A.O.; Alani, S.O.; Li, B.; Zeng, Q.-R.; Feng, W. Catalytic Removal of Selected Textile Dyes Using Zero-Valent Copper Nanoparticles Loaded on Filter Paper-Chitosan-Titanium Oxide Heterogeneous Support. *J. Polym. Environ.* **2021**. [[CrossRef](#)]
2. Zhang, Y.; Shi, J.; Xu, Z.; Chen, Y.; Song, D. Degradation of tetracycline in a schorl/ H_2O_2 system: Proposed mechanism and intermediates. *Chemosphere* **2018**, *202*, 661–668. [[CrossRef](#)]
3. Lin, Y.; Xu, S.; Li, J. Fast and highly efficient tetracyclines removal from environmental waters by graphene oxide functionalized magnetic particles. *Chem. Eng. J.* **2013**, *225*, 679–685. [[CrossRef](#)]
4. Su, Y.; Li, S.; Jiang, G.; Zheng, Z.; Wang, C.; Zhao, S.; Cui, D.; Liu, Y.; Zhang, B.; Zhang, Z. Synergic removal of tetracycline using hydrophilic three-dimensional nitrogen-doped porous carbon embedded with copper oxide nanoparticles by coupling adsorption and photocatalytic oxidation processes. *J. Colloid Interface Sci.* **2021**, *581*, 350–361. [[CrossRef](#)] [[PubMed](#)]
5. Oladipo, A.A.; Ifebajo, A.O. Highly efficient magnetic chicken bone biochar for removal of tetracycline and fluorescent dye from wastewater: Two-stage adsorber analysis. *J. Environ. Manag.* **2018**, *209*, 9–16. [[CrossRef](#)]
6. Anjali, R.; Shanthakumar, S. Insights on the current status of occurrence and removal of antibiotics in wastewater by advanced oxidation processes. *J. Environ. Manag.* **2019**, *246*, 51–62. [[CrossRef](#)] [[PubMed](#)]
7. Scaria, J.; Anupama, K.V.; Nidheesh, P.V. Tetracyclines in the environment: An overview on the occurrence, fate, toxicity, detection, removal methods, and sludge management. *Sci. Total Environ.* **2021**, *771*, 145291. [[CrossRef](#)] [[PubMed](#)]
8. Kumar, A.; Rana, A.; Sharma, G.; Naushad, M.; Dhiman, P.; Kumari, A.; Stadler, F.J. Recent advances in nano-Fenton catalytic degradation of emerging pharmaceutical contaminants. *J. Mol. Liq.* **2019**, *290*, 111177. [[CrossRef](#)]
9. Chen, H.; Liu, W.; Qin, Z. $\text{ZnO}/\text{ZnFe}_2\text{O}_4$ nanocomposite as a broad-spectrum photo-Fenton-like photocatalyst with near-infrared activity. *Catal. Sci. Technol.* **2017**, *7*, 2236–2244. [[CrossRef](#)]
10. Zhu, Y.; Liu, K.; Muhammad, Y.; Zhang, H.; Tong, Z.; Yu, B.; Sahibzada, M. Effects of divalent copper on tetracycline degradation and the proposed transformation pathway. *Environ. Sci. Pollut. Res.* **2020**, *27*, 5155–5167. [[CrossRef](#)]
11. Zou, S.; Xu, W.; Zhang, R.; Tang, J.; Chen, Y.; Zhang, G. Occurrence and distribution of antibiotics in coastal water of the Bohai Bay, China: Impacts of river discharge and aquaculture activities. *Environ. Pollut.* **2011**, *159*, 2913–2920. [[CrossRef](#)] [[PubMed](#)]

12. Gao, P.; Mao, D.; Luo, Y.; Wang, L.; Xu, B.; Xu, L. Occurrence of sulfonamide and tetracycline-resistant bacteria and resistance genes in aquaculture environment. *Water Res.* **2012**, *46*, 2355–2364. [[CrossRef](#)]
13. Yu, X.; Lin, X.; Li, W.; Feng, W. Effective Removal of Tetracycline by Using Biochar Supported Fe₃O₄ as a UV-Fenton Catalyst. *Chem. Res. Chin. Univ.* **2019**, *35*, 79–84. [[CrossRef](#)]
14. Wang, P.; Wang, L.; Sun, Q.; Qiu, S.; Liu, Y.; Zhang, X.; Liu, X.; Zheng, L. Preparation and performance of Fe₃O₄@hydrophilic graphene composites with excellent Photo-Fenton activity for photocatalysis. *Mater. Lett.* **2016**, *183*, 61–64. [[CrossRef](#)]
15. Murillo-Sierra, J.C.; Hernández-Ramírez, A.; Hinojosa-Reyes, L.; Guzmán-Mar, J.L. A review on the development of visible light-responsive WO₃-based photocatalysts for environmental applications. *Chem. Eng. J. Adv.* **2021**, *5*, 100070. [[CrossRef](#)]
16. Gouvêa, C.A.K.; Wypych, F.; Moraes, S.G.; Durán, N.; Nagata, N.; Peralta-Zamora, P. Semiconductor-assisted photocatalytic degradation of reactive dyes in aqueous solution. *Chemosphere* **2000**, *40*, 433–440. [[CrossRef](#)]
17. Trogadas, P.; Fuller, T.F.; Strasser, P. Carbon as catalyst and support for electrochemical energy conversion. *Carbon N. Y.* **2014**, *75*, 5–42. [[CrossRef](#)]
18. Das, S.; Ghosh, S.; Misra, A.J.; Tamhankar, A.J.; Mishra, A.; Lundborg, C.S.; Tripathy, S.K. Sunlight assisted photocatalytic degradation of ciprofloxacin in water using fe doped zno nanoparticles for potential public health applications. *Int. J. Environ. Res. Public Health* **2018**, *15*, 2440. [[CrossRef](#)]
19. Khiavi, N.D.; Katal, R.; Eshkalak, S.K.; Masudy-Panah, S.; Ramakrishna, S.; Jiangyong, H. Visible light driven heterojunction photocatalyst of cuo-cu2o thin films for photocatalytic degradation of organic pollutants. *Nanomaterials* **2019**, *9*, 1011. [[CrossRef](#)]
20. Yu, X.; Lin, X.; Feng, W.; Li, W. Effective Removal of Tetracycline by Using Bio-Templated Synthesis of TiO₂/Fe₃O₄ Heterojunctions as a UV-Fenton Catalyst. *Catal. Lett.* **2019**, *149*, 552–560. [[CrossRef](#)]
21. Kuang, Y.; Wang, Q.; Chen, Z.; Megharaj, M.; Naidu, R. Heterogeneous Fenton-like oxidation of monochlorobenzene using green synthesis of iron nanoparticles. *J. Colloid Interface Sci.* **2013**, *410*, 67–73. [[CrossRef](#)]
22. Wang, Y.; O'Connor, D.; Shen, Z.; Lo, I.M.C.; Tsang, D.C.W.; Pehkonen, S.; Pu, S.; Hou, D. Green synthesis of nanoparticles for the remediation of contaminated waters and soils: Constituents, synthesizing methods, and influencing factors. *J. Clean. Prod.* **2019**, *226*, 540–549. [[CrossRef](#)]
23. Liu, X.; Zhang, Q.; Yu, B.; Wu, R.; Mai, J.; Wang, R.; Chen, L.; Yang, S.-T. Preparation of Fe₃O₄/TiO₂/C Nanocomposites and Their Application in Fenton-Like Catalysis for Dye Decoloration. *Catalysts* **2016**, *6*, 146. [[CrossRef](#)]
24. Du, D.; Shi, W.; Wang, L.; Zhang, J. Yolk-shell structured Fe₃O₄@void@TiO₂ as a photo-Fenton-like catalyst for the extremely efficient elimination of tetracycline. *Appl. Catal. B Environ.* **2017**, *200*, 484–492. [[CrossRef](#)]
25. Feng, J.; Wang, Y.; Hou, Y.; Li, L. Hierarchical structured ZnFe₂O₄@RGO@TiO₂ composite as powerful visible light catalyst for degradation of fulvic acid. *J. Nanoparticle Res.* **2017**, *19*. [[CrossRef](#)]
26. Zhang, Y.F.; Qiu, L.G.; Yuan, Y.P.; Zhu, Y.J.; Jiang, X.; Xiao, J.D. Magnetic Fe₃O₄@C/Cu and Fe₃O₄@CuO core-shell composites constructed from MOF-based materials and their photocatalytic properties under visible light. *Appl. Catal. B Environ.* **2014**, *144*, 863–869. [[CrossRef](#)]
27. Zhao, W.; Wang, Y.; Yang, Y.; Tang, J.; Yang, Y. Carbon spheres supported visible-light-driven CuO-BiVO₄ heterojunction: Preparation, characterization, and photocatalytic properties. *Appl. Catal. B Environ.* **2012**, *115–116*, 90–99. [[CrossRef](#)]
28. Uthirakumar, P.; Devendiran, M.; Kim, T.H.; Kalaiarasan, S.; Lee, I.H. Fabrication of flexible sheets of Cu/CuO/Cu₂O heterojunction nanodisks: A dominant performance of multiple photocatalytic sheets under natural sunlight. *Mater. Sci. Eng. B Solid-State Mater. Adv. Technol.* **2020**, *260*, 114652. [[CrossRef](#)]
29. Yao, Y.; Lu, F.; Zhu, Y.; Wei, F.; Liu, X.; Lian, C.; Wang, S. Magnetic core-shell CuFe₂O₄@C₃N₄ hybrids for visible light photocatalysis of Orange II. *J. Hazard. Mater.* **2015**, *297*, 224–233. [[CrossRef](#)]
30. Akram, N.; Guo, J.; Ma, W.; Guo, Y.; Hassan, A.; Wang, J. Synergistic Catalysis of Co(OH)₂/CuO for the Degradation of Organic Pollutant Under Visible Light Irradiation. *Sci. Rep.* **2020**, *10*, 1–12. [[CrossRef](#)]
31. Kshirsagar, J.; Shrivastava, R.; Adwani, P. Preparation and characterization of copper oxide nanoparticles and determination of enhancement in critical heat flux. *Therm. Sci.* **2017**, *21*, 233–242. [[CrossRef](#)]
32. Ye, Y.; Wan, J.; Li, Q.; Huang, Y.; Pan, F.; Xia, D. Catalytic Oxidation of Dyeing Wastewater by Copper Oxide Activating Persulfate: Performance, Mechanism and Application. *Int. J. Environ. Res.* **2021**, *15*, 1–10. [[CrossRef](#)]
33. Mdletshe, L.S.; Makgwane, P.R.; Ray, S.S. Fabrication of bimetal CuFe₂O₄ oxide Redox-active nanocatalyst for oxidation of Pinene to renewable aroma oxygenates. *Nanomaterials* **2019**, *9*, 1140. [[CrossRef](#)]
34. Li, K.; Zhao, Y.; Janik, M.J.; Song, C.; Guo, X. Facile preparation of magnetic mesoporous Fe₃O₄/C/Cu composites as high performance Fenton-like catalysts. *Appl. Surf. Sci.* **2017**, *396*, 1383–1392. [[CrossRef](#)]
35. Sharma, K.; Raizada, P.; Hosseini-Bandegharai, A.; Thakur, P.; Kumar, R.; Thakur, V.K.; Nguyen, V.H.; Pardeep, S. Fabrication of efficient CuO/graphitic carbon nitride based heterogeneous photo-Fenton like catalyst for degradation of 2, 4 dimethyl phenol. *Process Saf. Environ. Prot.* **2020**, *142*, 63–75. [[CrossRef](#)]
36. Sun, Y.; Cho, D.-W.; Graham, N.J.D.; Hou, D.; Yip, A.C.K.; Khan, E.; Song, H.; Li, Y.; Tsang, D.C.W. Degradation of antibiotics by modified vacuum-UV based processes: Mechanistic consequences of H₂O₂ and K₂S₂O₈ in the presence of halide ions. *Sci. Total Environ.* **2019**, *664*, 312–321. [[CrossRef](#)]
37. Chai, F.; Li, K.; Song, C.; Guo, X. Synthesis of magnetic porous Fe₃O₄/C/Cu₂O composite as an excellent photo-Fenton catalyst under neutral condition. *J. Colloid Interface Sci.* **2016**, *475*, 119–125. [[CrossRef](#)] [[PubMed](#)]

38. Cordero-García, A.; Guzmán-Mar, J.L.; Hinojosa-Reyes, L.; Ruiz-Ruiz, E.; Hernández-Ramírez, A. Effect of carbon doping on WO₃/TiO₂ coupled oxide and its photocatalytic activity on diclofenac degradation. *Ceram. Int.* **2016**, *42*, 9796–9803. [[CrossRef](#)]
39. Zhao, Y.; Liu, L.; Shi, D.; Shi, X.; Shen, M. Performing a catalysis reaction on filter paper: Development of a metal palladium nanoparticle-based catalyst. *Nanoscale Adv.* **2019**, *1*, 342–346. [[CrossRef](#)]
40. Zhao, W.; Ma, W.; Chen, C.; Zhao, J.; Shuai, Z. Efficient Degradation of Toxic Organic Pollutants with Ni₂O₃/TiO₂-xBx under Visible Irradiation. *J. Am. Chem. Soc.* **2004**, *126*, 4782–4783. [[CrossRef](#)]
41. Wang, X.; Yu, J.C.; Chen, Y.; Wu, L.; Fu, X. ZrO₂-Modified Mesoporous Nanocrystalline TiO₂-xNx as Efficient Visible Light Photocatalysts. *Environ. Sci. Technol.* **2006**, *40*, 2369–2374. [[CrossRef](#)]
42. Wang, Q.; Wang, P.; Xu, P.; Li, Y.; Duan, J.; Zhang, G.; Hu, L.; Wang, X.; Zhang, W. Visible-light-driven photo-Fenton reactions using Zn_{1-1.5}Fe_xS/g-C₃N₄ photocatalyst: Degradation kinetics and mechanisms analysis. *Appl. Catal. B Environ.* **2020**, *266*, 118653. [[CrossRef](#)]
43. Gao, M.; Zhang, D.; Li, W.; Chang, J.; Lin, Q.; Xu, D.; Ma, H. Degradation of methylene blue in a heterogeneous Fenton reaction catalyzed by chitosan crosslinked ferrous complex. *J. Taiwan Inst. Chem. Eng.* **2016**, *67*, 355–361. [[CrossRef](#)]
44. Gao, N.; Lu, Z.; Zhao, X.; Zhu, Z.; Wang, Y.; Wang, D.; Hua, Z.; Li, C.; Huo, P.; Song, M. Enhanced photocatalytic activity of a double conductive C/Fe₃O₄/Bi₂O₃ composite photocatalyst based on biomass. *Chem. Eng. J.* **2016**, *304*, 351–361. [[CrossRef](#)]
45. Nazim, M.; Khan, A.A.P.; Asiri, A.M.; Kim, J.H. Exploring rapid photocatalytic degradation of organic pollutants with porous CuO nanosheets: Synthesis, dye removal, and kinetic studies at room temperature. *ACS Omega* **2021**, *6*. [[CrossRef](#)]
46. Ghasemi, H.; Aghabarari, B.; Alizadeh, M.; Khanlarkhani, A.; Abu-Zahra, N. High efficiency decolorization of wastewater by Fenton catalyst: Magnetic iron-copper hybrid oxides. *J. Water Process Eng.* **2020**, *37*, 101540. [[CrossRef](#)]
47. Benabbas, K.; Zabat, N.; Hocini, I. Facile synthesis of Fe₃O₄/CuO a core-shell heterostructure for the enhancement of photocatalytic activity under visible light irradiation. *Environ. Sci. Pollut. Res.* **2021**, *28*, 4329–4341. [[CrossRef](#)] [[PubMed](#)]
48. Tian, H.; Fan, H.; Dong, G.; Ma, L.; Ma, J. NiO/ZnO p–n heterostructures and their gas sensing properties for reduced operating temperature. *RSC Adv.* **2016**, *6*, 109091–109098. [[CrossRef](#)]
49. Takai, Z.I.; Mustafa, M.K.; Asman, S.; Sekak, K.A. Preparation and characterization of magnetite (Fe₃O₄) nanoparticles by sol-gel method. *Int. J. Nanoelectron. Mater.* **2019**, *12*, 37–46.
50. Yang, K.; Peng, H.; Wen, Y.; Li, N. Re-examination of characteristic FTIR spectrum of secondary layer in bilayer oleic acid-coated Fe₃O₄ nanoparticles. *Appl. Surf. Sci.* **2010**, *256*, 3093–3097. [[CrossRef](#)]
51. Wang, T.X.; Xu, S.H.; Yang, F.X. Green synthesis of CuO nanoflakes from CuCO₃·Cu(OH)₂ powder and H₂O₂ aqueous solution. *Powder Technol.* **2012**, *228*, 128–130. [[CrossRef](#)]
52. Yang, C.; Su, X.; Wang, J.; Cao, X.; Wang, S.; Zhang, L. Facile microwave-assisted hydrothermal synthesis of varied-shaped CuO nanoparticles and their gas sensing properties. *Sensors Actuators B Chem.* **2013**, *185*, 159–165. [[CrossRef](#)]
53. Halder, M.; Islam, M.M.; Ansari, Z.; Ahammed, S.; Sen, K.; Islam, S.M. Biogenic Nano-CuO-Catalyzed Facile C–N Cross-Coupling Reactions: Scope and Mechanism. *ACS Sustain. Chem. Eng.* **2017**, *5*, 648–657. [[CrossRef](#)]
54. Sun, X.; Gao, G.; Yan, D.; Feng, C. Synthesis and electrochemical properties of Fe₃O₄@MOF core-shell microspheres as an anode for lithium ion battery application. *Appl. Surf. Sci.* **2017**, *405*, 52–59. [[CrossRef](#)]
55. Taylor-Pashow, K.M.L.; Della Rocca, J.; Xie, Z.; Tran, S.; Lin, W. Postsynthetic Modifications of Iron-Carboxylate Nanoscale Metal–Organic Frameworks for Imaging and Drug Delivery. *J. Am. Chem. Soc.* **2009**, *131*, 14261–14263. [[CrossRef](#)] [[PubMed](#)]
56. Sun, B.; Li, H.; Li, X.; Liu, X.; Zhang, C.; Xu, H.; Zhao, X.S. Degradation of Organic Dyes over Fenton-Like Cu₂O-Cu/C Catalysts. *Ind. Eng. Chem. Res.* **2018**, *57*, 14011–14021. [[CrossRef](#)]
57. Xu, R.; Bi, H.; He, G.; Zhu, J.; Chen, H. Synthesis of Cu-Fe₃O₄@graphene composite: A magnetically separable and efficient catalyst for the reduction of 4-nitrophenol. *Mater. Res. Bull.* **2014**, *57*, 190–196. [[CrossRef](#)]
58. Jiang, D.; Wang, T.; Xu, Q.; Li, D.; Meng, S.; Chen, M. Perovskite oxide ultrathin nanosheets/g-C₃N₄ 2D-2D heterojunction photocatalysts with significantly enhanced photocatalytic activity towards the photodegradation of tetracycline. *Appl. Catal. B Environ.* **2017**, *201*, 617–628. [[CrossRef](#)]
59. Li, Y.; Cao, S.; Zhang, A.; Zhang, C.; Qu, T.; Zhao, Y.; Chen, A. Carbon and nitrogen co-doped bowl-like Au/TiO₃ nanostructures with tunable size for enhanced visible-light-driven photocatalysis. *Appl. Surf. Sci.* **2018**, *445*, 350–358. [[CrossRef](#)]
60. Zhuang, J.; Tian, Q.; Zhou, H.; Liu, Q.; Liu, P.; Zhong, H. Hierarchical porous TiO₂@C hollow microspheres: One-pot synthesis and enhanced visible-light photocatalysis. *J. Mater. Chem.* **2012**, *22*, 7036. [[CrossRef](#)]
61. Ma, T.Y.; Tang, Y.; Dai, S.; Qiao, S.Z. Proton-functionalized two-dimensional graphitic carbon nitride nanosheet: An excellent metal-/label-free biosensing platform. *Small* **2014**, *10*, 2382–2389. [[CrossRef](#)]
62. Zhang, W.; Bian, Z.; Xin, X.; Wang, L.; Geng, X.; Wang, H. Comparison of visible light driven H₂O₂ and peroxydisulfate degradation of norfloxacin using Co/g-C₃N₄. *Chemosphere* **2021**, *262*, 127955. [[CrossRef](#)]
63. Li, X.; Chen, C.; Zhao, J. Mechanism of Photodecomposition of H₂O₂ on TiO₂ Surfaces under Visible Light Irradiation. *Langmuir* **2001**, *17*, 4118–4122. [[CrossRef](#)]
64. Tang, J.; Wang, J. Fenton-like degradation of sulfamethoxazole using Fe-based magnetic nanoparticles embedded into mesoporous carbon hybrid as an efficient catalyst. *Chem. Eng. J.* **2018**, *351*, 1085–1094. [[CrossRef](#)]
65. Shao, Y.; Gao, Y.; Yue, Q.; Kong, W.; Gao, B.; Wang, W.; Jiang, W. Degradation of chlortetracycline with simultaneous removal of copper (II) from aqueous solution using wheat straw-supported nanoscale zero-valent iron. *Chem. Eng. J.* **2020**, *379*, 122384. [[CrossRef](#)]

66. Chen, Y.Y.; Ma, Y.L.; Yang, J.; Wang, L.Q.; Lv, J.M.; Ren, C.J. Aqueous tetracycline degradation by H₂O₂ alone: Removal and transformation pathway. *Chem. Eng. J.* **2017**, *307*, 15–23. [[CrossRef](#)]
67. Yu, L.; Wang, C.; Ren, X.; Sun, H. Catalytic oxidative degradation of bisphenol A using an ultrasonic-assisted tourmaline-based system: Influence factors and mechanism study. *Chem. Eng. J.* **2014**, *252*, 346–354. [[CrossRef](#)]
68. Yu, X.; Lin, X.; Feng, W.; Li, W. Enhanced catalytic performance of a bio-templated TiO₂ UV-Fenton system on the degradation of tetracycline. *Appl. Surf. Sci.* **2019**, *465*, 223–231. [[CrossRef](#)]
69. Wu, S.; Li, X.; Tian, Y.; Lin, Y.; Hu, Y.H. Excellent photocatalytic degradation of tetracycline over black anatase-TiO₂ under visible light. *Chem. Eng. J.* **2021**, *406*, 126747. [[CrossRef](#)]